4

MULTI-SCALE MODELLING PROGRAMME

This is a data intensive paradigm which addresses multiscale problems ranging from weather and climate, century-scale climate projections, space-based geodesy, computational geodynamics, surface processes and climate aspects from surface to ionosphere. The group continued development of system models and carried out the simulations of climate change, seasonal monsoon and climate under different aerosol scenarios, formulation of algorithms for analysis of simulations and deriving inferences in the field of climate sciences, lithosphere-hydrosphere-atmosphere-ionosphere interactions and computational geodynamics.

Inside

- Modelling aerosol-climate impacts
- Performance skill of state-of-the-art climate models in representing Indian summer monsoon
- Future changes in Indian summer monsoon from MRI ensemble projections
- Climate change projection of extreme events as projected by MRI AGCM3.2
- Future changes in rice yield over Kerala using climate change scenario from high resolution MRI AGCM3.2 model projection
- Aerosol mean monsoon relationship and interaction during extreme monsoon years
- Impact of aerosols on human health : Case study over the industrial area of Kochi, Kerala
- Aersol-Climate Effect
- Detecting aliasing free ionospheric disturbances using GPS
- Stress axis rotations at Andaman and Nicobar Islands after the 2004 Mw 9.2 Sumatra-Andaman earthquake.
- Seismogenesis at the Northern Wharton Basin, oceanic lithospheric stress and active shears
- Post-2004 seismogenic characteristics of Andaman Nicobar subduction zone
- Indian stable continental region earthquakes and source process characteristics

4.1 Modelling aerosol-climate impacts

Atmospheric aerosols can cause significant alteration in the energy balance of the atmosphere and the earth's surface by scattering and absorbing incoming solar radiation (direct effect), and strongly influence the processes of formation of clouds and precipitation (indirect effect). There are two types of indirect effect: 1) First Indirect effect or Twomey effect, 2) Second Indirect effect or Albrecht effect. The first indirect effect refers to an increase in aerosol concentration that can increase the reflectivity of the shallow clouds due to an increase in cloud condensation nuclei (CCN); whereas the total liquid water path is constant. In the second indirect effect due to an increase in CCN, the droplet number concentration increases and the effective radius decreases. These effects can increase the total liquid water path by reducing drizzle production. Aerosol properties are controlled by a combination of natural emissions, modification of the natural emissions by human activities such as land-use change, and anthropogenic emissions from biofuel combustion and early industrial processes. The aerosol concentrations were lower in the pre-industrial atmosphere than today.

We have ported and installed a coupled Earth System Model (NCAR-CESM) in our supercomputer ANANTA at CSIR-4PI, Bangalore. The atmospheric component of this model uses an active aerosol module. We conducted preliminary analysis of the simulated outputs of baseline simulations under two scenarios (pre-industrial and present-day). The performance in simulating the characteristics of Indian summer monsoon (ISM) is evaluated. The model well captures the ISM rainfall (ISMR) pattern in both scenarios. Over the Indian region, the difference shows a significant increase in rainfall in the present-day (Figure 4.1). This suggests that due to climate change, ISMR is increased in the present-day as compared to pre-industrial period. Also, long-term simulations are carried out using this model under different aerosol scenarios and are being analysed.

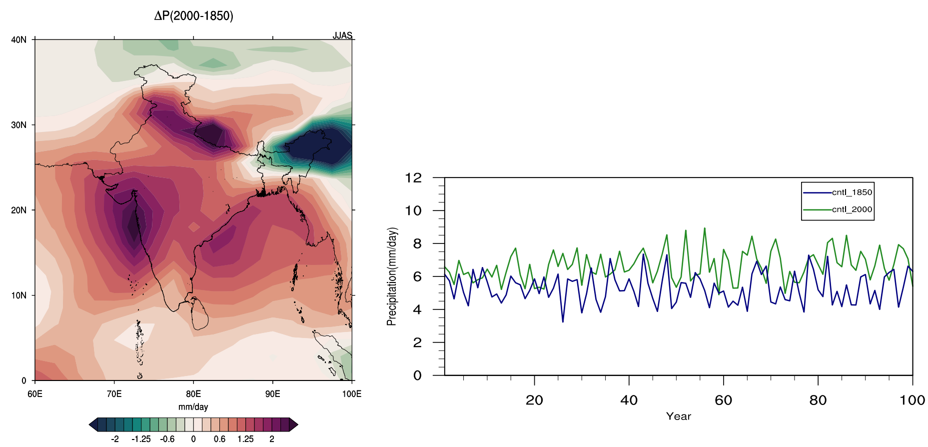

Figure 4.1: Change in JJAS rainfall climatology (100-year mean) between present-day (2000 control run) and pre-industrial period (1850 control run) over the Indian region (left). 100-year all-India JJAS rainfall for present-day (green line) and pre-industrial (blue line) period simulations (right).

4.2 Performance skill of state-of-the-art climate models in representing Indian summer monsoon

A correct representation of Indian summer monsoon (ISM) by models is a necessity owing to the impact it has on the economy of India. The processes within the monsoon system are very complex that even the current state-of-the-art general circulation models (GCMs) fail to capture the right representation of mean ISM. A realistic simulation of mean climatology by models can be considered as a yardstick in assessing the model's ability to simulate the processes involved in the dynamics of monsoon. Over the years, the models have improved in correctly simulating the mean monsoon climatology, but have severe drawbacks in simulating the variability that is associated with the ISM. The monsoon circulation is simulated fairly well by many of the GCMs but a detailed characteristic such as rainfall distribution is not well captured. Studies also found that model simulations are sensitive to parameterizations and most of the shortcomings appear near orographic regions.

Analysis of India's National Monsoon Mission (NMM) model, the Climate Forecast System (CFS) version 2 (CFSv2-CSIR-new) for hindcast runs for ISM season using 5 different initial conditions, viz., 21 April, 26 April, 01 May, 06 May and 11 May for a period of 39 years spanning 1979-2017 were done. The multimodel ensemble (MME) mean of the runs show underestimation of rainfall and a dry bias over India. A seasonal prediction system for all India rainfall with reasonable skill was thus found to be significantly below the potential limit of predictability.

Lack of reasonable high resolution was found to be a major reason for failure of models in rightly representing the ISM climatology. This necessitates for a model that simulates near to real ISMR climatology so that it may be used for future climate change projections and for local impact assessment studies. Meteorological Research Institute (MRI) Atmospheric GCM (AGCM) was developed with a horizontal grid size of ~20-km (Mizuta et al. 2006). The high horizontal resolution of the model helped in better representation of regional topographical effect and the physical processes therein. Moreover, atmosphere alone global model helped to make long-term climate simulations at very high resolution. The physical schemes within the 20-km MRI model were modified to improve the model performance, by inclusion of new parameterization scheme called Yoshimura scheme. Another version of MRI AGCM at ~60-km was also done to have more number of simulations with different physics schemes and initial conditions. A check on the skill of the above-mentioned models in simulating mean ISM climatology is made which shows that MRI MME has greater skill in simulating ISM climatology.

4.3 Future changes in Indian summer monsoon from MRI ensemble projections

The concentration of greenhouse gases is increasing at an alarming rate since the industrial revolution. This results in increased radiative forcing and associated rise in temperature of Earth's surface, causing large impact on the circulation patterns especially of monsoons. The possible changes in monsoon due to induced climate change requires attention because of the impact it can cause on the economy of the nation. Projection studies are possible with the help of General Circulation Models (GCMs). Many studies project an increased Indian summer monsoon (ISM) rainfall (ISMR) under future warming scenarios. The Meterological Research Institute (MRI) developed an Atmospheric GCM (AGCM) called MRI AGCM3.2 at very high resolution of ~60-km which has great skill in simulating present-day ISM climatology.

For future projection, the sea surface temperature and sea ice distribution are fed using time-slice mode. Here, the CMIP5 multi-model output is used as boundary data. The future boundary forcing is derived by perturbing the observed variables by an amount based on the results of CMIP5 model runs. The method thus decomposes observation data and CMIP5 model output into a combination of long-term mean, linear trend and interannual variability. Within CMIP5 model projections itself, Mizuta et al. 2014 followed a cluster analysis based on SST difference between historical and RCP8.5 scenario. Thus, 4 groups were derived with 3 groups clustered using SST difference method and one cluster formed by ensemble mean of all the clusters. The models were also projected under different RCP scenarios such as RCP2.6, RCP4.5, RCP6.0 and RCP8.5. Ensemble projections were made with MRI AGCM at 60-km resolution and by inclusion of Yoshimura parameterizations scheme because this configuration was found to reliably simulate the present-day ISM climatology.

The climate change projection of ISM using MRI 60-km model simulations with 4 future SST forcing and YS scheme under 4 different RCP scenarios yield that overall temperature over India increases by ~1.0^{o}C, ~2.0^{o}C, ~2.5^{o}C and ~4.0^{0}C and an overall increase in rainfall by ~0.12mm/day, ~0.43mm/day, ~0.67mm/day and ~1.0mm/day respectively for RCP2.6, RCP4.5, RCP6.0 and RCP8.5. The projected changes in mean rainfall shows an overall increase but not spatially coherent as that found for temperature. Change in rainfall shows an overall increase with a reduction over Western Ghats (WG) orographic region and parts of northeast India. The mechanism behind projected change is investigated and found that a combination of increased water vapour in the atmosphere along with increased low-level moisture transport into the subcontinent are the major contributing factors towards future enhancement of rainfall under RCP scenarios. Figure 4.2 shows the projected change in vertically integrated (upto 500hPa) moisture transport over Indian region. The increased transport into the interior of India for RCP8.5 is clearly seen.

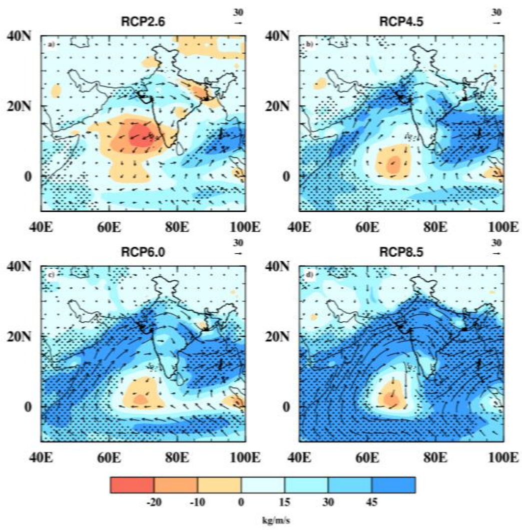

Figure 4.2 Projected future changes in VIMT up to 500hPa under a) RCP2.6, b) RCP4.5, c) RCP6.0 and d) RCP8.5 scenarios, with respect to the present day climate simulation over India. VIMT is given as vectors and the shading shows the magnitude of it. Values which are statistically significant at 95% level are stippled.

4.4 Climate change projection of extreme events as projected by MRI AGCM3.2

MRI AGCM3.2 in its 20-km and 60-km horizontal resolution were used extensively for studying the extreme events in the projected future climate. Extreme events such as floods, droughts, heat and cold waves are of great concern to the impact community and stakeholders. These extreme events were believed to have greater impact on economy than any change in the mean climate. With climate change, a drastic change in the frequency and intensity of extreme events are expected. This particularly affects developing countries like India with much gravity.

Analysis of extreme precipitation and temperature events were conducted using MRI AGCM3.2 at ~60-km horizontal resolution under future climate change scenarios, namely, RCP2.6, RCP4.5, RCP6.0 and RCP8.5. Variables such as daily maximum temperature, daily minimum temperature and daily accumulated rainfall were used for analysis due to their direct impact on population. Extreme event indices such as TX90p (number of days when daily maximum temperature exceeds 90th percentile), TN90p (number of days when daily minimum temperature exceeds 90th percentile) and R95p (number of days when daily precipitation exceeds 95th percentile) were calculated following methodology of ETCCDMI.
Analysis shows a uniform increase in number of days where daily maximum (minimum) temperature exceeds TX90p (TN90p) throughout the country. The number of warm nights is increasing much higher in magnitude than the increase in warm days. Warm days are projected to increase by ~10 days, ~ 12 days, ~17 days and ~31 days whereas warm nights are projected to increase by ~26 days, ~52 days, ~63 days and ~88 days respectively for RCP2.6, RCP4.5, RCP6.0 and RCP8.5. The projected change in extreme rainfall event (R95p) is not as uniform as that for temperature. For lower emission scenario, there is spatially an equal projection of increase and decrease of extreme rainfall event as shown in. Figure 4.3b. But, as the emission scenario increases, the percentage of grids with increased days of extreme rainfall increases from about 50% (RCP2.6) to about 90% (RCP8.5). The spatial distribution of changes in number of days with R95p for RCP8.5 is shown in Figure 4.3a.

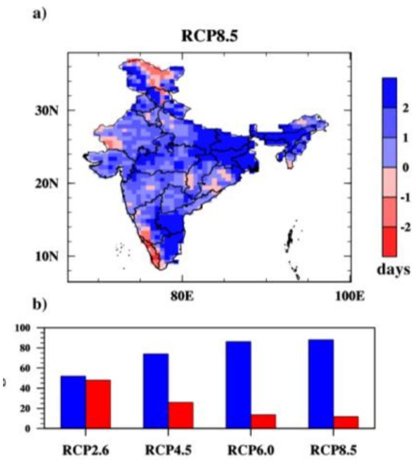

Figure 4.3 Projected future changes in number of days in JJAS with precipitation greater than 95th percentile (R95p). a) Spatial distribution of the changes for Rcp8.5 scenario and b) Percentage of grids with increased (decreased) number of days with rainfall greater (lesser) than R95p.

High resolution of model allows to study the regional changes in temperature and rainfall at various homogeneous zones. Uniform increase exists for both temperature and precipitation at all zones. For the temperature zones, increase in temperature was found to be 3.58^{o}C, 3.36^{o}C, 3.28^{o}C, 3.61^{o}C, 3.40^{o}C, 3.22^{o}C and 6.54^{o}C for interior peninsula, west coast, east coast, north central, northwest, northeast and western Himalaya respectively. For the rainfall homogeneous zones, the increase was found to be 1.04mm/day, 1.13mm/day, 0.98mm/day 1.42mm/day, 0.91mm/day, 1.75mm/day and 0.74mm/day for peninsular, west central, central northeast, northeast, northwest, northeast hilly regions and northern hilly regions respectively. The temperature indices also show the highest change over western Himalaya zone.

4.5 Future changes in rice yield over Kerala using climate change scenario from high resolution MRI AGCM3.2 model projection

The direct results that are obtained from climate models on a climate change perspective is what is addressed in most of the studies. The real value of such science can only be understood through a quantitative assessment of the impact of climate. A common manifestation of effect of climate change is in the change of agricultural output due to changes in climate variables that are responsible for growth and development of crops. Smart and adaptive agricultural practices need to be followed in order to tackle the problems relating to food and environment safety.

In a changing climate perspective, we get information of future climate scenario from general circulation models (GCMs). High resolution GCMs are preferred so as to derive information at a local scale. Rice is the major food consumed by more than half of the world's population. Its cultivation is determined by climate parameters such as daily temperature, rainfall, solar radiation and atmospheric carbon dioxide (CO_2) concentration. A single grid cell of the model is used for the study which corresponds to the location of rice cultivation over the Agricultural Research Station (ARS) Mannuthy, Kerala, located at 10^{o}32'N and 76^{o}20'E at an altitude of 22m above sea level.

Crop estimation was carried out using Crop Estimation through Resource and Environment Synthesis (CERES) model within DSSAT package. For the purpose of validation, field experiments were carried out during *Kharif* season of 2017 (May-November). Rice variety *Jyothi* was used for the purpose. The genetic coefficients of *Jyothi* were derived using intensive iteration process and the model has been calibrated for the rice variety and location under consideration.

Climate change information were derived from MRI AGCM3.2 at ~20-km resolution at the end of the 21st century under future climate scenario of RCP8.5. The input data for crop model are daily total precipitation, maximum surface air temperature, minimum surface air temperature and solar radiation. The MRI AGCM simulation for RCP8.5 scenario shows an overall increase intensification of summer monsoon rainfall and temperature over India, although with a reduction over Western Ghats (WG) region. This information is in accordance with the current trend of rainfall reduction over WG region. The location under consideration falls in this region as well.

For present day, the observed climatology (1994-2003) is fed for crop simulation. For future climate (2090-2099), the model output is bias corrected using delta change approach. Simulations to calculate potential yield were done with CO_2 concentration kept at constant value of 380ppm. Analysis of present-day and future yield of rice shows that panicle initiation day, anthesis day and physiological maturity day has shifted to an early period, by a decrease of ~4 days, ~7days and ~8 days respectively. A decrease in leaf area index is also seen from base period to future indicating a decrease in total biomass by ~957kg/ha. The decrease in grain yield is due to the differences in the environmental factors such as temperature, rainfall and solar radiation. An average rise of 2.8ºC of average temperature occurred from base period to future RCP8.5 scenario. A large increase of minimum temperature (2.8ºC-3.6ºC) was found to increase respiration losses leading to reduction in yield. A reduction in rainfall is also observed for future scenario which again caused for reduction in yield.

The study also found that yield is more if planting date is in the last week of July or first week of August, suggesting for a shift in the planting date for *Kharif* crop in the central zone of Kerala. Introduction of temperature tolerant, short duration varieties may be suggested for better water use efficiency.

4.6 Aerosol mean monsoon relationship and interaction during extreme monsoon years

Indian summer monsoon rainfall (ISMR) exhibits considerable yearly variation or interannual variation (IAV) despite the consistent seasonal reversal of circulation. ISMR is a coupled atmosphere-land-ocean phenomenon, where many factors such as sea surface temperature (SST), soil moisture, snow cover, cloud-radiative feed backs, El Nino-Southern Oscillation (ENSO), Equatorial Indian Ocean Oscillation (EQUINOO) etc. play significant roles. The strong association between the slowly emerging Sea Surface Temperature (SST) changes in the equatorial Pacific known as the ENSO and monsoon is demonstrated as increased tendency for deficit rainfall during El Niño and excess rainfall during its opposite phase, La Niña. Most of the ISMR are related to ENSO and/or EQUINOO modes. Droughts in 2002, 2004, 2009 and 2015 have occurred when El Niño and excess rainfall such as 2007 and 2011 have occurred when La Niña conditions prevailed in the Pacific. The largest ISMR deficit in recent decades was 2002 characterised by an intense and long break during July that lead to all-India rainfall being ~19% less than its long-term average and 2007 was an excess ISMR year. The AOD, convection and rainfall during 2002 deficit monsoon were compared with those during 2007 (Figure 4.4). Spatial distribution of AOD at the time of drought in 2002 showed that there were persistently high positive AOD anomalies over northern India and Indo-Gangetic plain and nearly opposite distribution was seen during the excess monsoon of 2007.
Typically, reduced (enhanced) rainfall was found to be associated with enhanced (reduced) AOD during deficit (excess) monsoon years. Seasonal AOD anomalies thus occur to be having a close-reverse relationship with the corresponding anomalies of rainfall. In fact, AOD anomalies were exceedingly positive in July of the deficit years of 2002 and 2004 when standardized ISMR anomalies were -4.07 and -1.25 respectively and were negative in July 2005 when ISMR anomaly was 1.51. Thus nearly inverse relationship between AOD and rainfall was seen in the anomalies on monthly scale as well. This is consistent with the

perceptive that increased washout of aerosols take place in rainy conditions, and aerosol life times are longer in arid conditions.

Aerosols can participate in cloud and rainfall processes in different ways; as CCN/IN or as absorbing particles readjusting solar energy as thermal energy. As aerosols are effective CCN/IN, their variability is expected to modulate the cloud optical properties such as cloud effective radius (CER) and cloud optical thickness (COT). The seasonal analysis shows that anomalies are significantly lower in 2002 while AODs are higher, implying an association between aerosols and clouds, and possibly an evidence for the indirect radiative effect of aerosols on clouds. These results emphasize the fact that when aerosols become abundant, they can decrease the cloud effective radius.

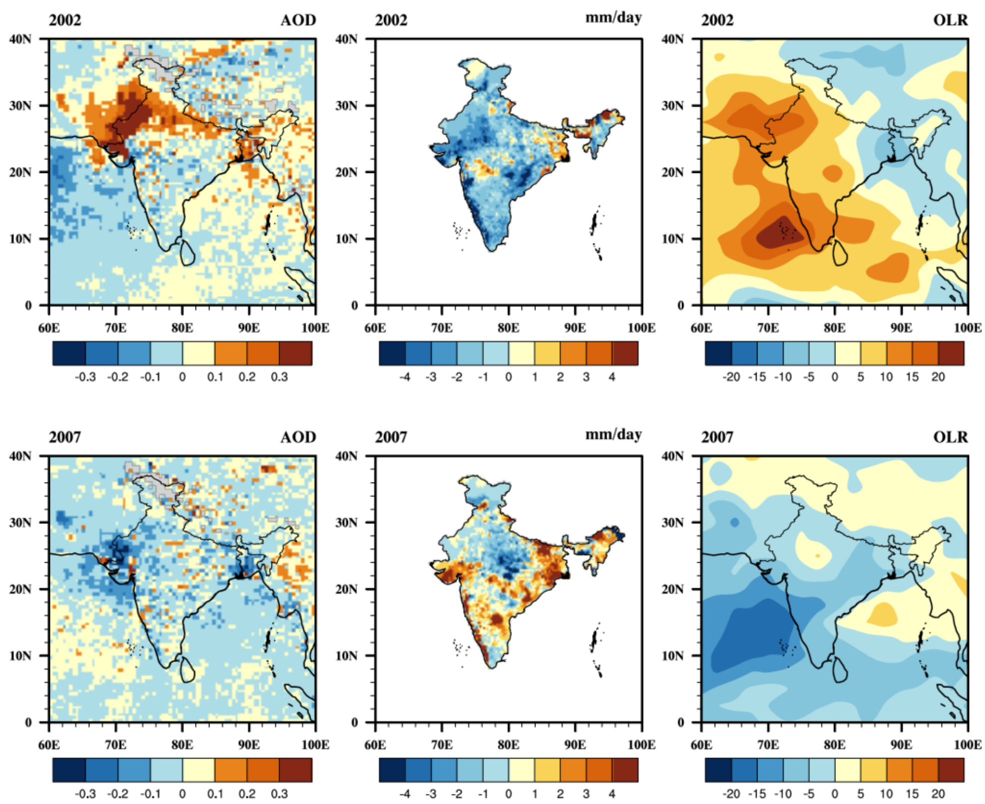

Figure 4.4 Seasonal (JJAS) anomalies of AOD, rainfall and OLR in a drought (upper panels) and excess rainfall year (lower panels).

4.7 Impact of aerosols on human health: Case study over the industrial area of Kochi, Kerala

The quality of environment have strong linkage with human health. Particulate matter pollution is one of the serious threats that we are facing now a days. The exposure of particulate matter pollution can cause number of health problems such as cardiovascular diseases, respiratory problems, increases in hospital admission, doctor and emergency room visits, absences from school and work, mainly for with pre-existing heart or lung disease, older people and children. The Global Burden of Diseases (GDB) study of 2017 shows that 76.8% of Indians are exposed to higher level of PM concentration, which is above the national standard (40 μg/m^3) on ambient air pollution. Particulate matter pollution has been increased significantly over the past decade in India. According to comprehensive

Environmental Pollution Index (CEPI), Kochi has been identified as one of the critically polluted area.

The analysis of particulate matter pollution over Kochi from 2010 to 2018 for different station shows varying trend pattern for each station for different season. This investigation reveals Eloor is the most polluted place in Kochi all over the year. Eloor is the main industrial zone in Kochi consist of more than 247 industries. The other industrial zones, Irumpanam and Kalamassery also shows increasing trend, but not much higher as Eloor. The non-industrial stations like Vytilla and M.G Road shows high value of increasing trend during post-monsoon months. This indicates particulate matter pollution is not only the mainconcern over the industrial regions but also in residential and other places of Kochi. The increase in the particulate matter concentration over these places is due to the increase in the construction activities.

Investigation of impact of particulate matter pollution on human health over Eloor municipality, reveals the main cause of death of people is due to cardiovascular disease, bronchitis and asthma.The analysis of death registered in Eloor municipality since 2010 to 2018 shown in Figure 4.5. The total number of death registered during the study period is 1563, out of this 41.39 % died due to cardiovascular disease, 26.10% due to different reasons comes under the category others, 21.17 % died due to bronchitis and asthma, 7.35 % due to cancer and 0.63% due to other respiratory illness. The analysis of hospital admission records from ESCI hospital, Eloor also shows a constant increase the hospital admission due to unspecified acute lower respiratory, cardiovascular diseases, chronic obstructive pulmonary disease during the study period of from 2014 to 2018. All these analysis indicates particulate matter pollution is a serious matter of concerns to the life of people in Eloor.

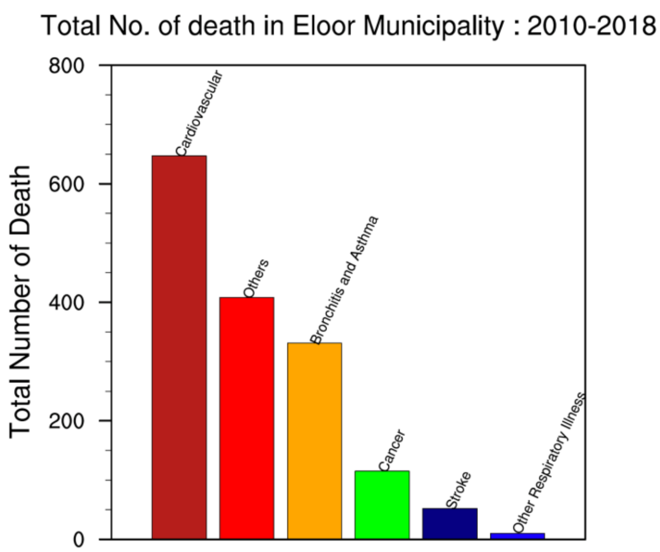

Figure 4.5 Total number of death occurred in Eloor municipality from 2010 to 2018.

4.8 Aerosol-Climate Effect

The indirect effect of radiative forcing in warm cloud can be either due to increase in droplet number (increased Cloud Condensation Nucleii) or changing precipitation efficiency. Cloud Condensation Nucleii (CCN) are mostly formed by aerosols with diameter 0.1-1 µm. Aerosols play an important role in global mean radiative forcing as the concentration of particles is highly variable (short lifespan). Though aerosol radiative forcing is known to affect Indian Summer Monsoon Rainfall (ISMR), the mechanism is not yet fully. Hence, it is important to understand the role of aerosol radiative forcing on ISMR to improve the understanding of complex mechanism associated with it.

We set up a coupled Earth System Model (NCAR-CESM v1.2) to understand the role of aerosol concentration on the SW monsoon rainfall variability over Indian subcontinent during industrial period. Two model simulations were performed: one is the present day simulation (CONTROL_2000) covering industrial period and second one is the simulation covering pre-industrial period (CONTROL_1850). Figure 4.6 shows averaged rainfall for SW monsoon period (June-September) from the present-day simulation and the difference of this from pre-industrial simulation. The model captured rainfall patterns very well for both the runs (not shown). Difference between two simulations show that the precipitation has increased during industrial period over central India. Aerosol parameters except dust (AOD-DUST) show a significant increase in industrial period. Dust aerosol is found to be decreased over Indian subcontinent during industrial period.

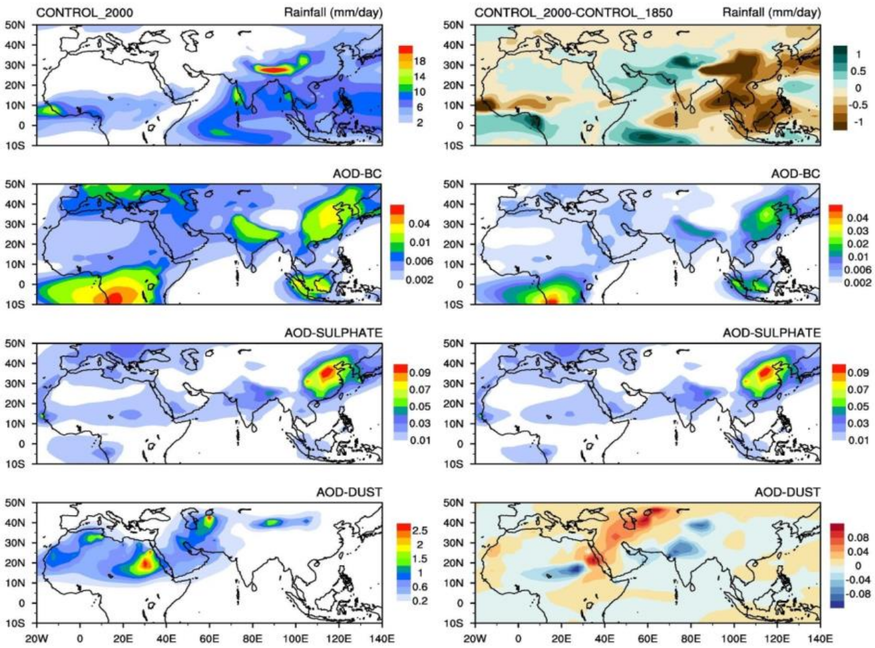

Figure 4.6 Model outputs of present-day simulation (CONTROL_2000) for Rainfall, BC (AOD-BC), Sulphate (AOD-SULPHATE) and dust (AOD-DUST) aerosols. All parameters were averaged for JJAS. Right panel shows the difference between present-day and pre-industrial (CONTROL_1850) simulations.

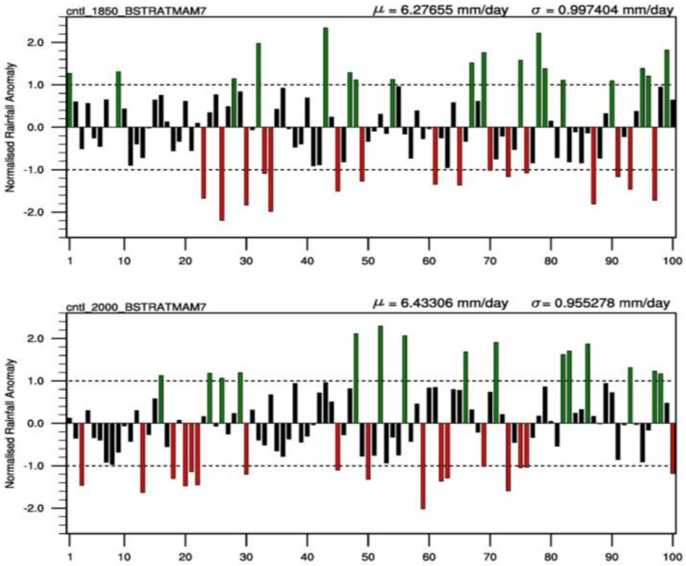

Figure 4.7 Normalised rainfall anomaly (JJAS) for both pre-industrial (CONTROL_1850) and present-day (CONTROL_2000) simulations. Green bars indicate flood years and red bars indicate drought years. Normal years are represented by black bars. X-axis shows year.

We also calculated the normalised monsoon rainfall (JJAS) for both pre-industrial and present day runs to identify the flood and drought years (Figure 4.7). There is an increase (0.15mm/day) in the mean JJAS rainfall for the present day run. During pre-industrial period 18 (16) flood (drought) are noted which is 15 (17) during industrial period. Difference of flood and drought composites for pre-industrial and present day runs are shown in Figure 4.8 to show the spatial variability. Spatial patterns are similar in both the runs with increased amplitude during pre-industrial run.

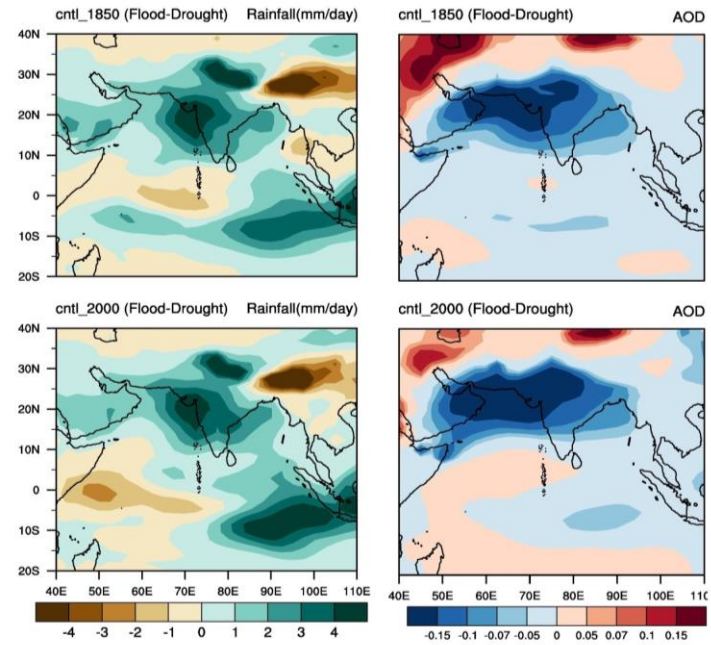

Figure 4.8 Difference of composite map of flood years and draught for both pre-industrial and present-day run.

4.9 Detecting aliasing free ionospheric disturbances using GPS

Ionospheric disturbances (ID) observed using GPS are widely used to study the dynamics of the ionosphere and impact of space weather on the ionosphere. Further, measured IDs are also used to study the impact of space weather on radio communication and satellite based navigation. However, the IDs are conventionally derived as Rate of ionospheric Total Electron Content (ROT) suffer aliasing due to the unaccounted spatial gradient associated with the non-uniform spatial sampling. We proposed an improvised algorithm – Spatio-Periodic Levelling Algorithm (SPLA) – to remove such aliasing. Efficiency of the proposed algorithm SPLA was validated using theoretical simulations (Figure 4.9) and observations carried out at ~13.5 million ionospheric pierce points observed during 2015 St. Patrick's day geomagnetic storm. Spatio-temporal, and SNR analyses of simulated and observed IDs reveal that the proposed algorithm efficiently removes aliasing, expands area of coverage up to 65%, and increases average SNR to 99.5%.

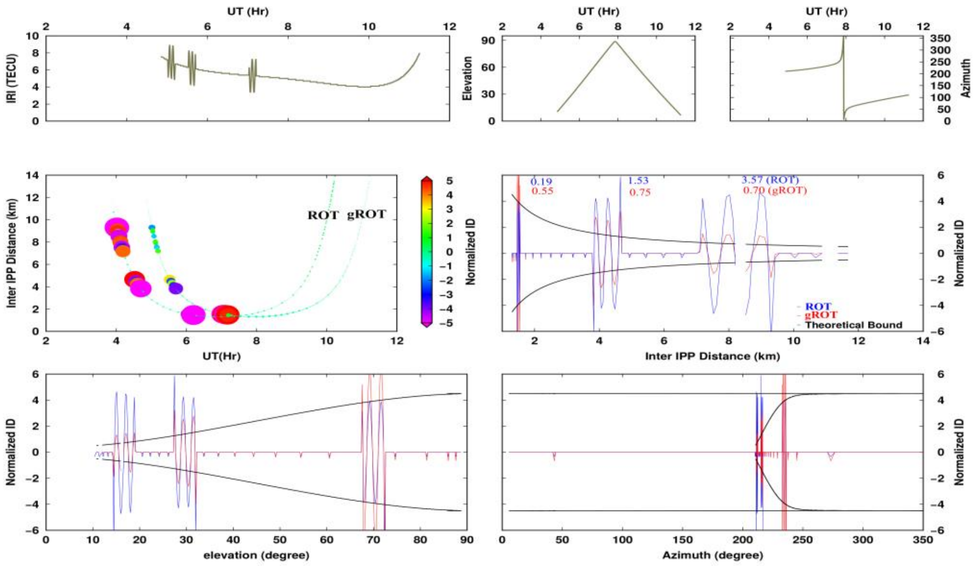

Figure 4.9 (Top left) Synthetic TEC along DUBO29 on March 17, 2015 super-imposed with simulated IDs. (Top middle and right) Elevation and azimuth of GPS satellite PRN29 tracked by GPS receiver at DUBO. (Middle left) Normalized ROT and gROT as function of time and inter-IPP distance. gROT is shifted by 1 h for clarity. (Middle right) Normalized IDs with respect to inter-IPP distance. Values printed over the IDs are relative deviation of the simulated IDs from the theoretical bound. (Bottom) Variation of normalized IDs with respect to elevation and azimuth.

4.10 Stress axis rotations at Andaman and Nicobar Islands after the 2004 Mw 9.2 Sumatra-Andaman earthquake.

There is a huge spurt in seismicity all along the Sumatra-Andaman subduction zone (SASZ), post the Mw 9.2 2004 Sumatra-Andaman earthquake which show an along-arc spatio-temporal variability in faulting style, stress regimes and deformational mechanisms. It is reported that the great subduction zone earthquakes would cause rotation of the lithospheric principal stress axes and has been largely observed after mega-thrust ruptures. Similar characteristic nature of rotation of maximum compressional axis (σ1) and minimum compressional axis (σ3) is observed along the SASZ after the 2004 megathrust earthquake where the inter-seismic values of σ1 increased from ~15-21^0 to about 30 to 40^0. We observed a back rotation in all the segments, except in the North Andaman segment. These back-rotations are catching-up the pre-seismic trends with some along-arc differences. Co-seismically the σ1 steepened and later it tends to return to the pre-seismic trends at the early post-seismic period (e.g., North Sumatra and Nicobar). The post-earthquake σ1 at Nicobars rotated further in the later post-seismic phase and presently favours extension, whereas North Sumatra continues towards pre-seismic trend with shallow plunge. On the other hand at Northern segments, the σ1 does not reach back towards the inter-seismic counterparts. The rapid rotation here is due to the combined effect of the post-seismic activities like the afterslip in addition to the co-seismic stress relief, which was high at the Little Andaman and Nicobar (~80%) and low at the North Sumatra (~60%) and North Andaman (~50%) (Figure 4.10).

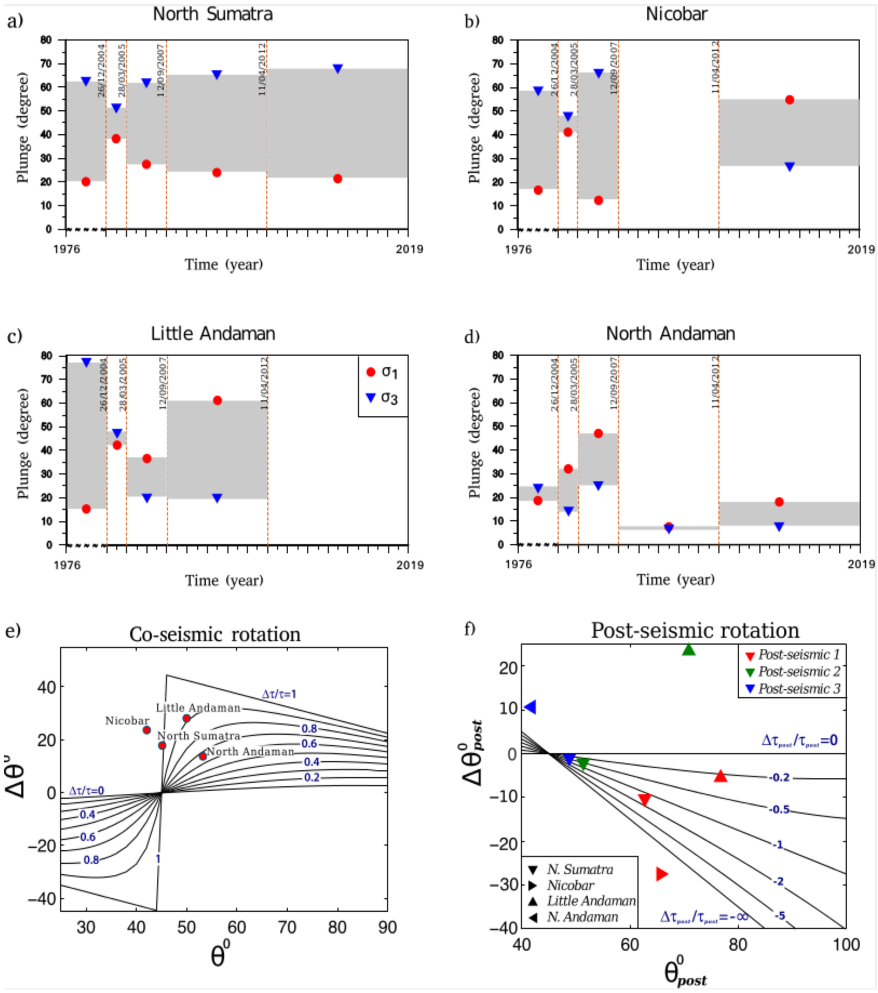

Figure 4.10 Rotation of minimum and maximum compressional axes at the Andaman Nicobar region after the 2004 Mw 9.2 Sumatra-Andaman megathrust earthquake.

4.11 Seismogenesis at the Northern Wharton Basin, oceanic lithospheric stress and active shears

The Wharton Basin (WB), part of the world's most actively deforming oceanic lithosphere, the Indo-Australian plate, has hosted several large intraplate earthquakes. The characteristic deformational mechanisms in the WB is mostly of strike-slip earthquakes and it is believed that these earthquakes are associated with the N-S oriented left-lateral active fracture zones, parallel to the 90^{0}E ridge. Several studies have been carried out to understand the seismogenic characteristics of this region. But still questions and uncertainties concerning the seismogenesis within the WB tectonics still exist including characteristics of active faults in the subducting Indian plate, extent of seismic slips in the oceanic lithosphere, whether it source within the 600^{0}C isotherm or beyond that and its linkage with tectonic stress. We studied the kinematic source process models of three large earthquakes in the northern WB. We found these events are better explained by faulting on E-W oriented active shear structures in this region. The centroid depths of these earthquakes lie within the 600^{0}C isotherm but the seismic slip extends by rupturing the crust and mantle and a case which reaches up to the 750^{0}C isotherm. The analysis of stress regime at the north WB showed a depth-wise variations in stress field at this region indicates shallow oblique-normal faulting and deeper oblique-reverse, indicating plate bending effects or slip-partitioning effects having direct control on the ongoing tectonics (Figure 4.11).

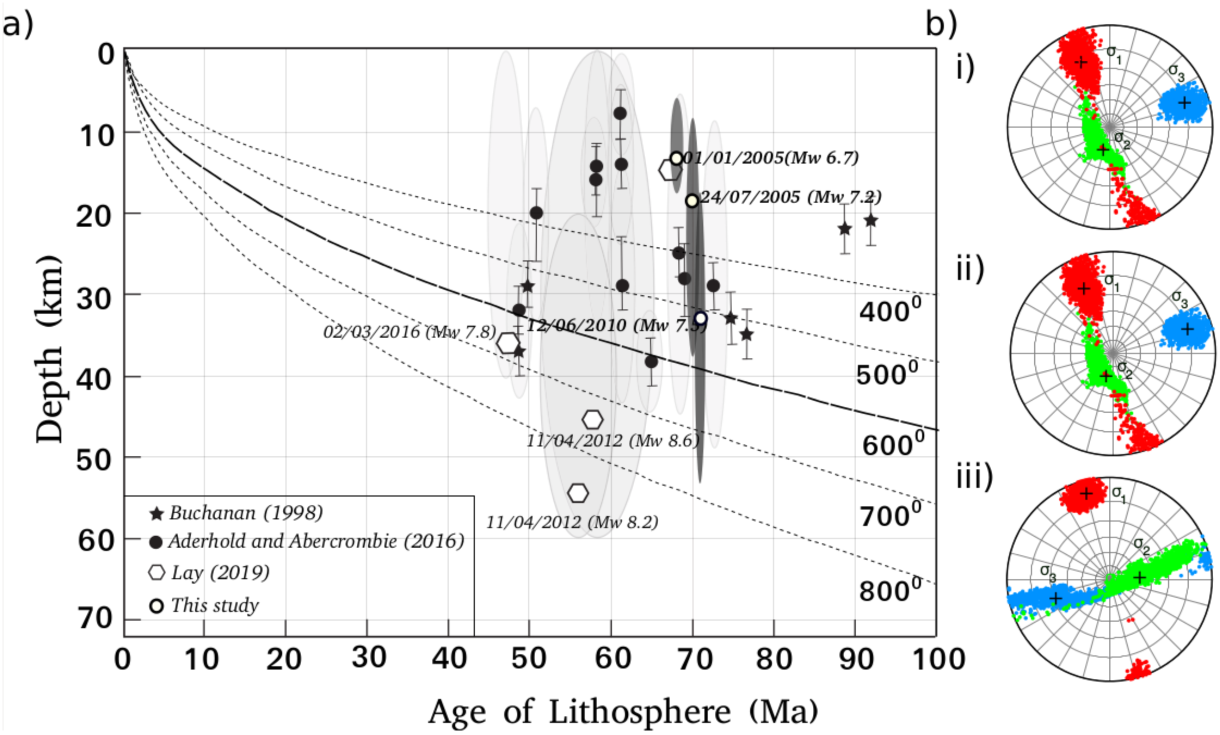

Figure 4.11 a) Seismogenic depth of Indian Ocean earthquakes. b) Modelled stress fields of Northern Wharton Basin.

4.12 Post-2004 seismogenic characteristics of Andaman Nicobar subduction zone

It is globally observed that after a megathrust rupture shallow normal faulting earthquakes occur, in the seaward of the subducting slab, till a transition depth, below which the sinking plate shows thrust earthquakes or becomes aseismic. This style of faulting, as deeper compression below a shallow extension, represents strain build-up within the bending slab, as it descends into the upper mantle. Unlike the global tendencies observed so far, the post-megathrust rupture seismogenesis at the outer-rise and further seaward of the

Sumatra-Andaman margin represents a mixture of faulting mechanisms include normal, thrust as well as strike-slip events which denote a more complex pattern of deformation along this margin. Analysis of active faulting characteristics of the three large earthquakes (2 normal and 1 strike-slip) at the outer-rise region of the north and Little Andamans show that the earthquakes rupture in near margin parallel direction. We suggest that the outer-rise regions of the North, South and Little Andaman regions are actively deforming due to slab bending effects. In addition, large amount of strike-slip earthquakes with margin parallel compressional axis are observed at the northern Andaman region where the oblique convergence is maximum, which reduces towards south. This suggests the possible influence of northward drag of Indian plate stresses for the strike-slip earthquakes there and the possibility of partitioning of slip within the subducting Indian slab, post 2004 megathrust rupture (Figure 4.12).

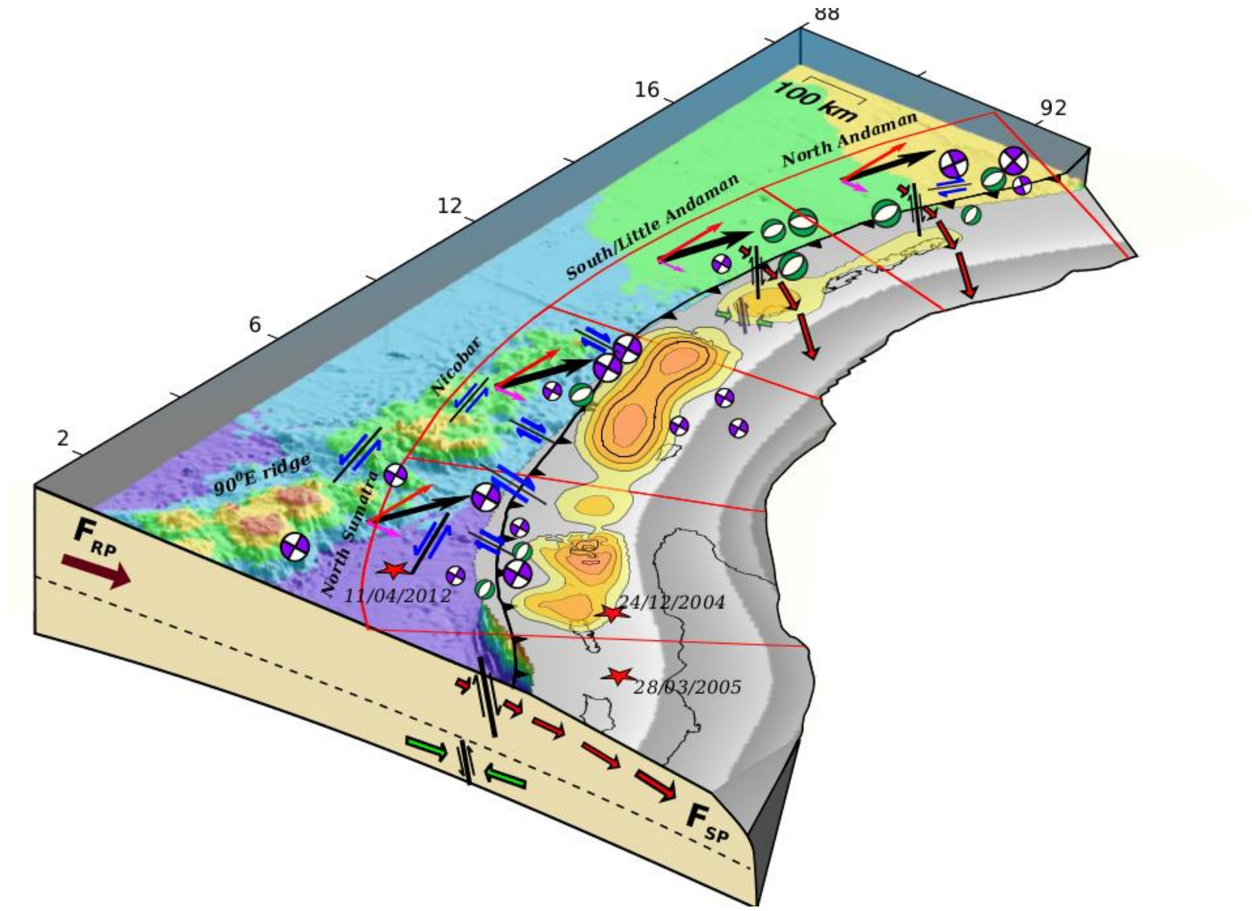

Figure 4.12 Schematic representation of active tectonic deformation of the Andaman Nicobar margin post 2004 Mw 9.2 Sumatra Andaman earthquake.

4.13 Indian stable continental region earthquakes and source process characteristics

Global distribution of shield area earthquakes indicates that the stable continental regions (SCR) are exposed to destructive events. The case of Indian subcontinent, is no different by hosting many moderate to large earthquakes in the past and is one of the most seismically active SCR in the world. It is widely believed that these events occurred by the reactivation of paleo-rifts or weak faults at shallow depths. We analyzed kinematic source process models and the evolution of rupture and stress drop of the three Indian SCR earthquakes occurred in the instrumental era, the 1993 Mw 6.2 Latur, 1997 Mw 5.8 Jabalpur and the 2001 Mw 7.6 Bhuj. This study shows that, these events do have a compact zone of singular asperity breakage within the Indian crust, where Bhuj and Jabalpur events have their rupture restricted within the lower crustal regions, whereas Latur event ruptured a shallow crustal asperity. These events exhibited comparatively higher stress drop estimates, indicating fracturing at newer faults than on the existing features. The high difference in the energy based stress-drop and seismic moment based stress-drop estimates and large spatial-variations in slip and stress-drops within the Bhuj slip region point towards a heterogeneous slip plane with possibility of varying maturity and roughness (Figure 4.13).

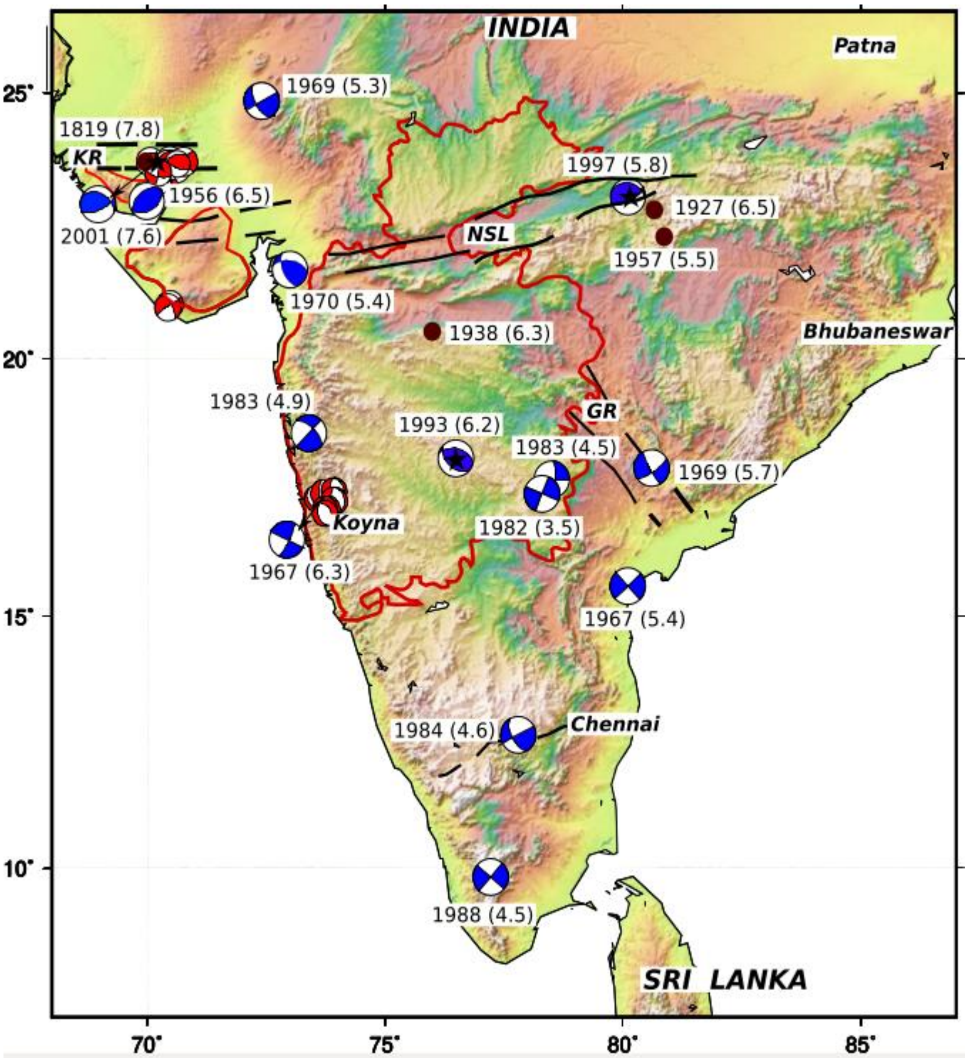

Figure 4.13 Map of earthquake faulting mechanism distribution of major Indian stable continental region earthquakes. KR: Kachchh Rift, GR: Godawari Rift, NSL: Narmada-Son lineame